Experimental and computational analysis of toughness anisotropy in an AA2139 Al-alloy for aerospace applications

Thilo F. Morgeneyer, Jacques Besson, Henry Proudhon, M.J. Starink, I. Sinclair

▶ **To cite this version:**

Thilo F. Morgeneyer, Jacques Besson, Henry Proudhon, M.J. Starink, I. Sinclair. Experimental and computational analysis of toughness anisotropy in an AA2139 Al-alloy for aerospace applications. International conference on fracture, Jul 2009, Ottawa, Canada. 10 p. hal-00822196

HAL Id: hal-00822196

https://minesparis-psl.hal.science/hal-00822196

Submitted on 14 May 2013

HAL is a multi-disciplinary open access archive for the deposit and dissemination of scientific research documents, whether they are published or not. The documents may come from teaching and research institutions in France or abroad, or from public or private research centers.

L'archive ouverte pluridisciplinaire **HAL**, est destinée au dépôt et à la diffusion de documents scientifiques de niveau recherche, publiés ou non, émanant des établissements d'enseignement et de recherche français ou étrangers, des laboratoires publics ou privés.

Experimental and computational analysis of toughness anisotropy in an AA2139 Al-alloy for aerospace applications

T.F. Morgeneyer[1,3], J. Besson[1], H. Proudhon[1], M.J. Starink[2] and I. Sinclair[2]
[1] *Mines ParisTech, Centre des matériaux, CNRS UMR 7633, BP87 91003 Evry Cedex, France*
[2]*School of Engineering Sciences, University of Southampton, Southampton, UK*
[3]*Alcan Centre de Recherches de Voreppe, BP 27, 38341 Voreppe Cedex, France*

Abstract

Fracture toughness anisotropy of AA2139 (Al-Cu-Mg) in T351 and T8 conditions has been investigated via mechanical testing of smooth and notched specimens of different geometries, loaded in the rolling direction (L) or in the transverse direction (T). Fracture mechanisms were investigated via SEM and synchrotron radiation computed tomography (SRCT). Contributions to failure anisotropy are identified with: (i) anisotropic initial void shape and growth, (ii) plastic behaviour including isotropic/kinematic hardening and plastic anisotropy, and (iii) nucleation at a 2nd population of 2nd phase particles leading to coalescence via narrow crack regions. A model based in part on the Gurson-Tvergaard-Needleman approach is constructed to describe and predict deformation behaviour, crack propagation and, in particular, toughness anisotropy. Model parameters are fitted using microstructural data and data on deformation and crack propagation for a range of small test samples. Its transferability has been shown by simulating tests of large M(T) samples.

1 Introduction

Aluminium sheet is widely used for lightweight high performance structures, particularly within the transport sector. For the design of structures it is crucial to control mechanical properties, such as fracture toughness [1]. In practice, the transferability of toughness trends between small test pieces (such as Kahn tear tests [2]) to large panel M(T) specimens [3] is an important aspect in optimising materials performance for components. One materials issue that is particularly difficult to take account for in predicting toughness performance of large panels is the anisotropy of toughness in sheet.

Possible sources of toughness anisotropy in wrought aluminium sheet are numerous. One possible cause is plastic anisotropy developed during rolling, this may be identified with the energy dissipated during fracture depending on the local load level and consequently on the loading direction for anisotropic materials [4]. A second cause of toughness anisotropy is related to the anisotropic shape and distribution of defects introduced by material processing [5,6,7,8,9,10,11,12,13], whilst a third cause may be identified with prior pre-straining as such materials are often stress relieved after quenching [14].

Several models incorporating the above mechanisms have been proposed in the literature. Models are often based on the micromechanical Gurson model [15] and

its “standard” extension proposed by Tvergaard and Needleman (so called GTN model) [16]. Introducing plastic anisotropy can be easily done by replacing the von Mises stress in the expression of yield surface given by the GTN model by any anisotropic stress measure. Recently proposed macroscopic models [17,18,19] can be used as shown in [4]. Models accounting for initial void shape and shape evolution have been developed for prolate and oblate voids by Gologanu and co-workers [9,10]. This approach has a major limitation however: cavities are assumed to be, and remain, axisymmetric so that the model must be adapted in case of non-axisymmetric loading [12]. Models based on the GTN approach that simultaneously account for ductile damage and kinematic hardening have been proposed in the literature but with limited verification or testing against experimental data [20].
In the present study fracture toughness anisotropy of AA2139 (Al-Cu-Mg) is investigated experimentally via mechanical testing of smooth and notched samples of different sizes, charcterisation of the microstructure involving synchrotron radiation computed tomography (SRCT) and fractographic assessment also involving an SRCT study of arrested cracks [21]. A novel computational assessment of toughness anisotropy is reported here briefly [22], based on the GTN-approach and that accounts for the found material characteristics. The parameter identification has been performed using microstructural data and experimental results from small samples and the behaviour of large M(T) samples is successfully predicted using these parameters.

2 Material and experimental methods

• *Material*: AA2139 sheet was supplied by Alcan CRV with a thickness of 3.2mm in an industrial T351 condition, *i.e.* solution treated, stretched and naturally aged. The composition ranges are given in Table 1.
The material has subsequently been tested in two different conditions (see Table 2), T351 (*i.e*. as-received), and after a further ageing treatment approximating a standard T8 for this alloy. In the interest of brevity, we will refer to the T351 condition as simply ‘T3’ for the purpose of this paper.

Si	Fe	Cu	Mn	Mg	Ag	Ti	Zn
<= 0.1	<= 0.15	4.5 - 5.5	0.20 - 0.6	0.20 - 0.8	0.15 - 0.6	<= 0.15	<=0.25

Table 1: Composition limits of alloy AA2139 in weight % (adapted after [21])

T351 (as received)	T8
Solutionise, quench, 2% stretch in rolling direction, naturally age	The as-received material, additionally aged at 175 °C for 16 hours

Table 2: Conditions tested for AA2139 sheet (adapted after [21])

Mean pore dimensions (3D Feret measurements) are given in Table 3 for the three material processing directions (rolling direction (L), long transverse direction (T), short-transverse direction (S)). Pore content determination was influenced by the choice of the grey scale threshold, with Table 3 identifying the corresponding

error levels. 3D Voronoi tessellation [23] of the void distribution revealed average cell dimensions of 45µm, 48µm and 50µm in the L, T and S direction respectively, *i.e.* indicative of near-neighbour separation distances in these directions [24]. Consistent with these figures the Voronoi cell aspect ratios for cells around the pores are found to be close to unity. The particles were seen to be aligned as stringers, with stringer dimensions of the order of 15-30µm (*cf.* 1-10µm in direction T and 1-6µm in direction (S)). The volume fraction of coarse intermetallic particles, and the Feret dimensions of Voronoi cells around pores and intermetallic particles obtained from SRCT data is given in Table 3. Pores were seen to be closely linked with the intermetallic distribution, with a large proportion being associated with one or more intermetallic particles. However, no significant distribution anisotropy for pores and particles can be detected between T and L direction using average Voronoi cell dimensions (see Table 3). Figure 1 shows an FEG-SEM backscattered electron image of the material in the L-T plane, highlighting the presence of dispersoid particles that are predominately elongated in the L direction.

	Porosity			**Intermetallic particles**		
f_v in %	0.34 with a variation of ±10% when setting extreme grey values.			0.45 ±15% (standard error based on repeat measurements at different locations and magnifications).		
	Mean Feret dimensions of pores in µm			Mean Feret dimensions of Voronoi cells around 2nd phase particles and pores in µm		
	L	T	S	L	T	S
	7.6	5.4	4.5	23	24	25

Table 3: Porosity and intermetallic particle content, dimensions and distribution of the AA2139 alloy. (Pore content and pore Feret dimension and was reported previously [24]) (adapted after [21])

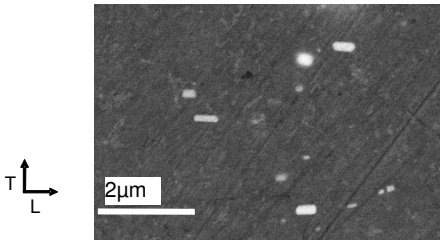

Figure 1: FEG-SEM image in backscattered mode (20kV) of in the L-T plane showing dispersoids (adapted after [21])

• *Mechanical testing:* Four types of test specimen have been utilized (see Figure 2): smooth flat tensile specimens, notched flat tensile specimens (EU2), Kahn tear test specimens and large M(T) panels. Two orientations of loading in the sheet plane have been investigated for all samples: L and T. In the Kahn and M(T) specimens loaded in the L direction, cracks will clearly propagate in the T direction; these tests are referred to as L-T, and vice versa for T-L designated tests. At least two tests have been performed in each condition/direction combination, whilst for the M(T) sample only one test has been performed per

condition/direction. For technical reasons, M(T) tests for T-L loading have only been carried out for the T3 condition.

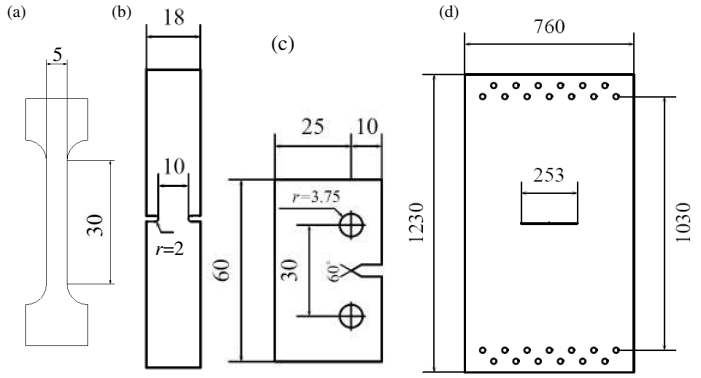

Figure 2: Specimen geometries for: (a) tensile samples (b) EU2 samples (c) Kahn tear test samples (d) M(T) samples (all dimensions in mm) (adapted after [21])

The SRCT sample scanning conditions and sample preparation procedures are described in [2,3,4,21]

3 Experimental results

In this section the mechanical testing results on samples of different sizes are given; for the sake of brevity the results of the simulations described in the section 6 are also plotted. In the T3 condition (Figure 3(a)) tensile behaviour is anisotropic. For testing in the L direction yield strength, as well as loads for a given elongation, are higher than the T direction, with a yield strength difference ~80 MPa, average flow stress difference ~15 MPa and a small difference in ultimate tensile strength. The difference in initial tensile curve shape is thought to be mostly due to the prestraining by ~2% that the material has undergone. The through-thickness deformation is essentially the same for the two testing directions however, whilst the slope of the through-thickness variation *vs.* applied strain is close to 0.5 (*i.e.* as for isotropic behaviour).

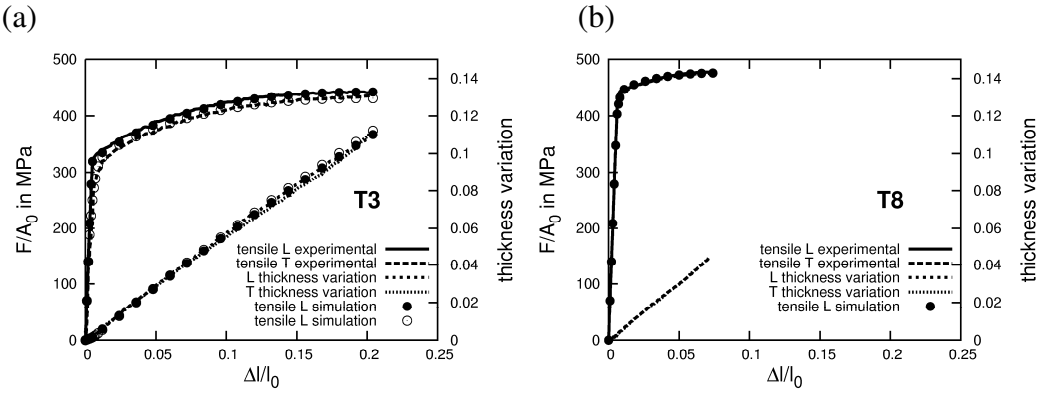

Figure 3: Tensile tests experimental and simulation for naturally aged and artificially aged (T3 and T8) material (adapted after [22])

For the material in the T8 condition (Figure 3(b)) tensile deformation curves in the different loading directions, as well as the corresponding through-thickness deformation curves, are essentially identical. Overall it is seen that the ageing treatment has lead to higher yield strength and reduced ductility compared to the T3 condition.

Figure 4 shows the nominal stress vs. crack mouth opening displacement (CMOD) curves for EU2 tests in the L and T directions for the T3 and the T8 condition. Figure 4(a) shows anisotropy in the load curve for the T3 material only, whilst final failure occurs at similar opening displacements.

Consistent with the tensile tests, the L and T loading of EU2 samples in the T8 condition (Figure 4(b)) do not show significantly different plastic behaviour. However, final failure in the L direction occurs at ~0.1mm higher opening displacement than the T.

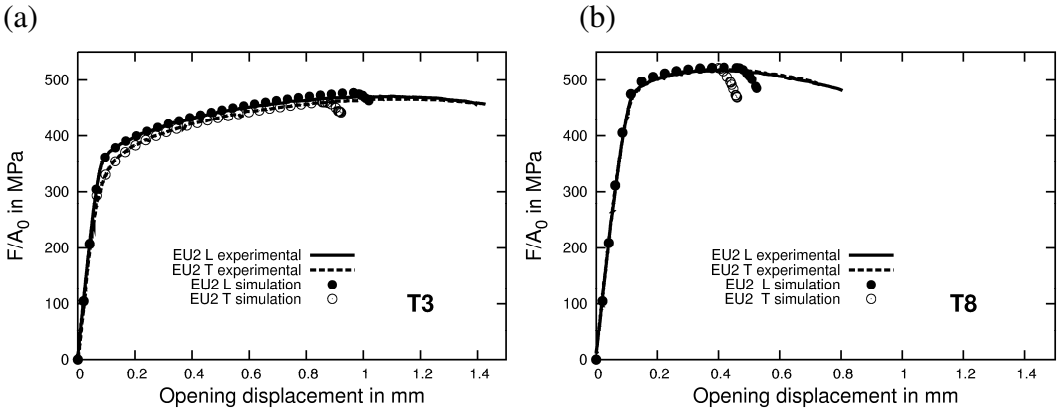

Figure 4: EU2 tests experimental and simulation for naturally aged and artificially aged (T3 and T8) materials (adapted after [22])

Figure 5 shows the results of the Kahn tear tests in terms of force F divided by the initial ligament area A_0 as a function of the CMOD, along with the crack length as a function of the CMOD for L-T and T-L testing for the T3 and T8 conditions. For the T3 material (Figure 5 (a)) the maximum nominal load is smaller for the T-L testing (*i.e.* indicating a lower initiation toughness). The load differences between the T-L and L-T samples are even higher in the propagation region and crack growth is faster in the T-L test orientation than in the L-T. For the T8 material (Figure 5 (b)) the nominal load is very similar for both sample orientations up to the maximum load. Nominal stresses in the propagation region are however substantially lower for the T-L sample than for the L-T sample and crack growth is faster for the T-L test compared to the L-T. Initiation and propagation toughness are substantially lower for the T8 material than for the T3.

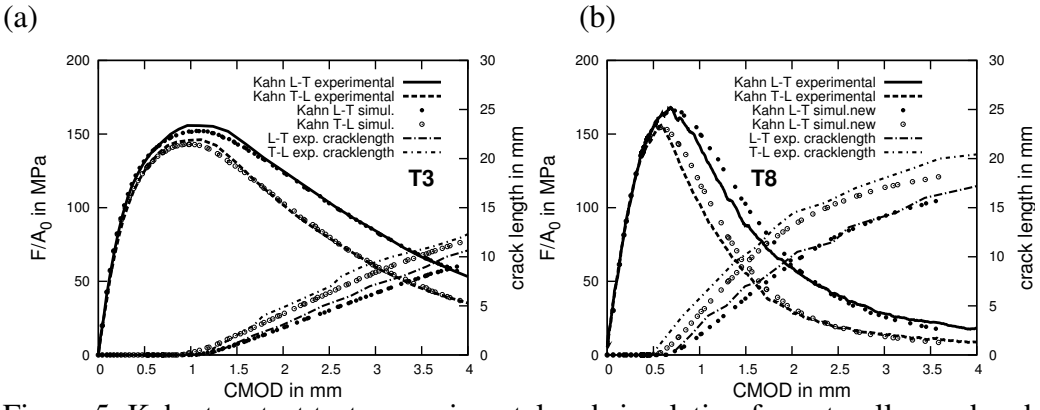

Figure 5: Kahn tear test tests experimental and simulation for naturally aged and artificially aged (T3 and T8) materials (adapted after [22])

Figure 6 shows the results of M(T) tests for (a) the T3 condition (T-L loading only) and (b) the T8 condition and both loading directions. Strong toughness anisotropy can be identified for the T8 material. The maximum load of the L-T sample is ~24% higher than for the T-L sample, which is clearly higher than the corresponding anisotropy measured for the Kahn tear tests (8%, see Figure 5).

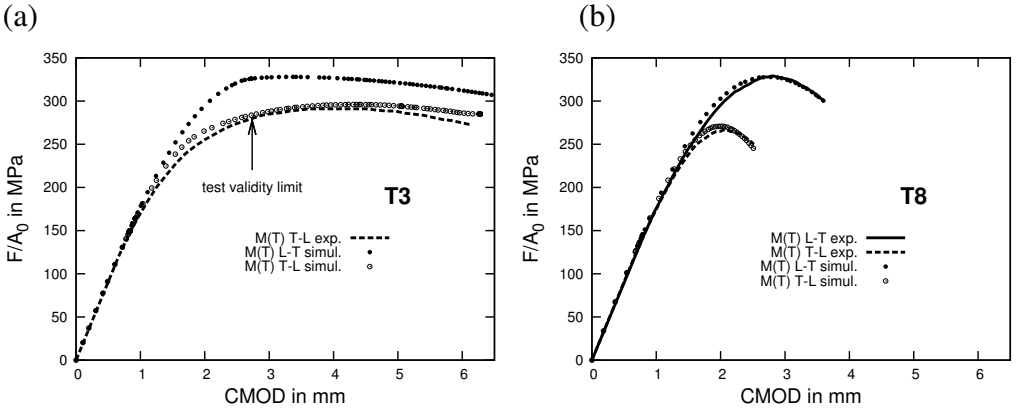

Figure 6: M(T) test results for simulation and experiment for naturally aged and artificially aged (T3 and T8) materials (adapted after [22])

4 Fractography

The fracture of Kahn tear test samples typically starts with a macroscopically flat triangular region, oriented normal to the loading direction [25], with the crack subsequently turning into a slanted crack with an angle of ~45º with respect to the loading direction, this is then maintained during further crack propagation (also see [25]). The reader is referred to [21] for corresponding fractographic images. For all test conditions the fracture surface in the flat triangular region was seen to be dominated by dimples associated either with coarse particles or initial porosity. The voids appear to have mainly coalesced via impingement. For the T-L samples the surface morphology was more obviously directional, with void chains apparent on the fracture surface, parallel to the material rolling direction.

In the propagation region (slanted crack growth), fracture was still dominated by coarse voiding, however areas containing fine dimples were also observed, consistent with shear decohesion (also called void sheeting [26]). The features on the fracture surfaces of the T-L and L-T samples appeared similar but aligned stringers are again more apparent in the T-L sample.
SRCT studies of arrested cracks in the fracture initiation region are presented in detail in [21]. It has been identified that already in the region of high stress triaxiality coalescence may occur through regions of narrow opening linked to void nucleation at a small population of small 2nd phase particles such as shown in Figure 7.

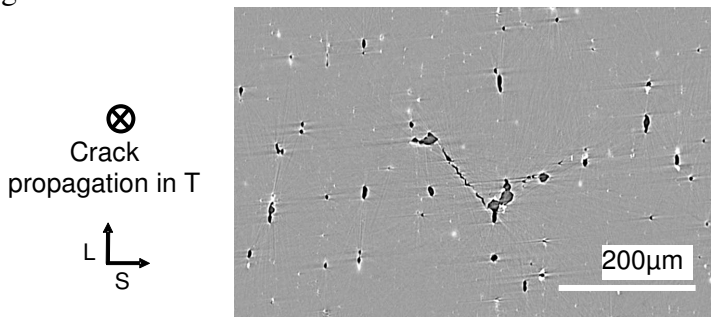

Figure 7: 2D section of SRCT results of the crack tip of an arrested crack (before reaching peak load) of a T-L Kahn tear test sample in T8 condition

5 Model

In the experimental study it could be identified that the T3 material displays i) anisotropic initial void shape and growth, (ii) plastic behaviour including isotropic/kinematic hardening and plastic anisotropy, and (iii) nucleation at a 2nd population of second phase particles leading to coalescence via narrow crack regions. The T8 material did not exhibit kinematic hardening or plastic anisotropy. A model based in part on the Gurson-Tvergaard-Needleman (GTN) approach has been constructed to describe and predict deformation behaviour, crack propagation, and, in particular, toughness anisotropy. The model is described in full detail in [22]. The mean stress in the GTN yield function has been replaced by a weighted sum of the stresses along the 3 materials processing directions to account for anisotropic void growth.
Kinematic hardening caused by material prestrain has been accounted for using the formulation used by Lemaitre and Chaboche [27] which is incorporated in the GTN approach as suggested in [20]. Plastic anisotropy is accounted for using the approach suggested by Bron and Besson [17]. Finally the nucleation of damage is modeled using an expression suggested by Chu and Needleman [28].

6 Simulation

To account for anisotropic initial void shape and growth, weighting parameters were fitted using unit cell calculation results. Average dimension measured via SRCT in the alloy were used for the initial void shape in the unit cell calculations.

Parameters related to isotropic/kinematic hardening and plastic anisotropy were determined via simulation of the prestrain of 2% and subsequent simulation of the tensile and EU2 tests using an automatic optimization procedure. The results are shown in Figure 3 and 4. Using these parameters, simulations of Kahn tear tests for different directions have been carried out. Curve shape up to maximum experimental load, and also fracture anisotropy, could be predicted. However, fracture loads were too high using physically meaningful mesh sizes [29]. To address we idenitify the use of anisotropic critical strains to represent nucleation of damage at small 2nd population of second phase particles, such as dispersoids, reducing predicted fracture loads. The critical strains have been determined via trial and error simulations of Kahn tear tests. The results are shown in Figure 5. The premature predicted fracture of the EU2 samples (see Figure 4) using the critical strains may be linked to the fact that stress triaxiality is lower for EU2 samples than for Kahn samples and the found critical strains may only be valid for high stress triaxality. Using the obtained parameters the fracture of M(T) samples has been simulated and a good fit has been obtained showing the transferability of the results obtained with small samples and microstructural data to large samples (see Fig 6). The detailed parameter identification procedure is further outlined in [22].

7 Conclusions

Mechanical tests on smooth and notched specimen of different sizes have been carried out in two loading directions for T3 and T8 materials. It has been identified that T3 material isotropic and kinematic hardening and also some plastic anisotropy play a role. The T8 material is plastically isotropic. Fractography of Kahn samples has revealed fracture mechanisms linked to coarse voiding and shear decoheasion, especially in the propagation region. Some alignment of dimple stringers is prevalent on the T-L sample fracture surfaces in the rolling direction. SRCT studies of arrested cracks in the crack initiation region have revealed the unexpected presence of coalescence through narrow regions that can be linked to void nucleation at a small population of 2nd phase particles. Anisotropic initial void shape has been identified through SRCT studies of the as-received material. No significant anisotropic average distribution of pores and particles could be measured using Feret dimensions around Voronoi cells. Dipsersoid particles were seen to be elongated in the L direction of the material.
A model based on the GTN approach has been developed incorporating (i) anisotropic initial void shape and growth, (ii) plastic behaviour including isotropic/kinematic hardening and plastic anisotropy, and (iii) nucleation at a 2nd population of 2nd phase particles leading to coalescence via narrow crack regions. For the first time a model for kinematic hardening accounting for ductile damage has been successfully applied to structures. A new simple method to account for initially anisotropic void shape and growth is suggested that is easier to implement than other approaches and is not restricted to axisymmetric cavities. Parameters have been fitted on mechanical testing results of small samples. It has been found that neither kinematic hardening nor anisotropic void shape can fully

describe the fracture toughness anisotropy. It is proposed to account for coalescence and nucleation at a 2nd population of small 2nd phase particles via nucleation at different critical strains for the different material directions which may be linked to the anisotropic shape and/or distribution of small 2nd phase particles such as dispersoids. Simulation of fracture of large M(T) samples using the found parameters shows that this method is suitable to predict fracture toughness anisotropy fitted on small samples.

Acknowledgements

The authors would like to acknowledge Alcan CRV for financial support and material supply, and Frédéric Bron and Bernard Bès for technical discussion. We would also like to thank Jean-Yves Buffière and Elodie Boller for support in micro-computed tomography.

References

[1] A. Cho, B. Bes, Damage Tolerance Capability of an Al-Cu-Mg-Ag Alloy(2139), Mater Sci Forum 519-521 (2006) 603-608
[2] ASTM-international, Standard B 871 - 01. 2001.
[3] ASTM-international, Standard E 561 - 98. 1999
[4] F. Bron , J. Besson, Simulation of the ductile tearing for two grades of 2024 aluminum alloy thin sheets, Eng Fract Mech 73 (2006) 1531-1552.
[5] A.A. Benzerga, J. Besson, A. Pineau, Anisotropic ductile fracture: Part I: experiments, Acta Mater 52 (2004) 4623-4638
[6] D. Dumont, A. Deschamps, Y. Brechet, On the relationship between microstructure, strength and toughness in AA7050 aluminum alloy, Mat Sci Eng A 356 (2003) 326-336.
[7] D. Steglich, W. Brocks, J. Heerens, T. Pardoen, Anisotropic ductile fracture of Al 2024 alloys, Eng Fract Mech 75 (2008) 3692-3706
[8] A.A. Mir, D.C. Barton, T.D. Andrews, P. Church, Anisotropic ductile failure in free machining steel at quasi-static and high strain rates. Int J Fract 133 (2005) 289-302
[9] M. Gologanu, J.B. Leblond, J. Devaux, Approximate models for ductile metals containing nonspherical voids - case of axisymmetric oblate ellipsoidal cavities, Trans ASME J Eng Mater Technol 116 (1994) 290-297.
[10] M. Gologanu, J.B. Leblond, J. Devaux, Approximate models for ductile metals containing non-spherical voids, Case of axisymmetric prolate ellipsoidal cavities J Mech Phys of Solids 41 (1993) 1723-1754.
[11] T. Pardoen, J.W. Hutchinson, Extended model for void growth and coalescence, J Mech Phys Solids 48 (2000) 2467-2512
[12] A.A. Benzerga, J. Besson, A. Pineau, Anisotropic ductile fracture: Part II: theory, Acta Mat 52 (2004) 4639-4650
[13] T. Pardoen, J.W. Hutchinson, Micromechanics-based model for trends in toughness of ductile metals, Acta Mat 51 (2003) 133-148

[14] Y. Bao, R. Treitler, Ductile crack formation on notched Al2024-T351 bars under compression-tension loading, Mater Sci Eng A 384 (2004) 385-394
[15] A.L. Gurson, Continuum theory of ductile rupture by void nucleation and growth: part 1 yield criteria and flow rules for porous ductile media, J Eng Mater Technol 99 (1977) 2-15
[16] V. Tvergaard, A. Needleman, Analysis of the cup-cone fracture in a round tensile bar, Acta Metall 32 (1984) 157-169
[17] F. Bron, J. Besson, A yield function for anisotropic materials Application to aluminum alloys, Int J Plasticity 20 (2004) 937-963
[18] A.P. Karafillis, M.C. Boyce, General anisotropic yield criterion using bounds and a transformation weighting tensor, J Mech Phys Solids 41 (1993) 1859-1886
[19] F. Barlat, H. Aretz, J.W. Yoon, M.E. Karabin, J.C. Brem, R.E. Dick, Linear transfomation-based anisotropic yield functions, Int J of Plasticity 21 (2005) 1009-1039
[20] J. Besson, C. Guillemer-Neel, An extension of the Green and Gurson models to kinematic hardening, Mechanics of Materials 35 (2003) 1-18
[21] T.F. Morgeneyer, J. Besson, H. Proudhon, M.J. Starink, I. Sinclair, Analysis of toughness anisotropy in AA2139 Al-alloy sheet; part I: experiments, Acta Mat, submitted
[22] T.F. Morgeneyer, J. Besson, M.J. Starink, I. Sinclair, Analysis of toughness anisotropy in AA2139 Al-alloy sheet; part II: model and simulations, Acta Mat, submitted
[23] N. Yang, J. Boselli, I. Sinclair, Simulation and quantitative assessment of homogeneous and inhomogeneous particle distributions in particulate metal matrix composites, J Microsc 201 (2001) 189-200
[24] T.F. Morgeneyer, M.J. Starink, I. Sinclair, Evolution of voids during ductile crack propagation in an aluminium alloy sheet toughness test studied by synchrotron radiation computed tomography, Acta Mat 56 (2008) 1671-1679.
[25] F. Bron , J. Besson, A. Pineau, Ductile rupture in thin sheets of two grades of 2024 aluminum alloy Mater. Sci Eng A A 380 (2004) 356-364
[26] W.M. Jr Garrison, N.R. Moody, Ductile fracture J. Phys. Chem. Solids 48 (1987) 1035-1074
[27] J. Lemaitre, J. Chaboche, Mechanics of Solid Materials. Cambridge University Press, Cambridge, 1990
[28] C.C. Chu, A. Needleman. Void nucleation effects in biaxially stretched sheets. Transactions of the ASME. Journal of Engineering Materials and Technology 102 (1980) 249-56.
[29] A.S. Gullerud, X. Gao, R.H. Dodds, R. Haj-Ali . Simulation of ductile crack growth using computational cells: numerical aspects, Eng Fract Mech 66 (2000) 65-92